P9.67

# PRECIPITATION OBSERVATIONS FROM POLARIMETRIC SARS OF THE COSMO-SKYMED SATELLITE CONSTELLATION

L. Baldini*, N. Roberto, E. Gorgucci, Institute of Atmospheric Sciences and Climate – CNR, Roma, Italy
J. Fritz, Colorado State University, Fort Collins CO 80523
V. Chandrasekar, Colorado State University,Fort Collins and Finnish Meteorological Institute, Helsinki, Finland

## 1. INTRODUCTION

In Synthetic Aperture Radar (SAR) images, precipitation results in both backscatter enhancement and attenuation of surface backscattering. Effect of attenuation is quite evident in convective cells observed by SAR operating at X-band (X-SAR). Due to the anisotropy of many hydrometeors, propagation and backscattering effects depend on polarization and polarimetric SAR can detect therefore different precipitation signatures especially if local incidence angle is far from vertical. A further effect is determined by the inherent Doppler spectrum of precipitation that degrades the nominal azimuth resolution, which however remains better than that provided by current space borne precipitation radars. COSMO SkyMed (Constellation of Small Satellites for Mediterranean basin Observation, CSK) is an Italian Space Agency (ASI) mission based on a constellation of four satellites equipped with a SAR at X-band with polarimetric capabilities (Agenzia Spaziale Italiana 2007). An attractive feature of the full constellation is the short revisiting time (that is the capability to image a given area also using different conditions such as varying SAR look angle) of the order of a few hours. This paper focuses on the analysis of images collected by the SARs of the COSMO SkyMed constellations in the presence of precipitation using the dual-polarization mode called HH-VV Ping Pong. In this mode, SAR operates in HH for a fraction of the synthetic aperture, and then VV is used. Therefore, HH and VV returns are not coherent with each other and only copolar returns can be analyzed. Images were collected in 2010, when the constellation was composed of three satellites. Quasi-coincident volumetric observations from ground-based radar can be used to estimate the components due to precipitation (namely attenuation and precipitation backscattering) that determine SAR returns in precipitation, providing a valuable tool to support interpretation of SAR images with precipitation. Polarimetric SAR observations were scheduled in 2010 on regions where operational or research weather radars were available, namely Piedmont (Italy) Tampa Bay (Florida, US), and Helsinki (FI) where the Bric della Croce C-band dual polarization radar, two NEXRAD radars and the University of Helsinki Kumpula radar were running, respectively. At the moment, the dataset of CSK images collected in precipitation is composed by one image in Piedmont and 4 images in Tampa Bay, out of 62 images collected. This paper, after a brief illustration of the model describing precipitation effects in polarimetric SAR returns, introduces the methodology to reconstruct SAR observations based on radar measurements. Specific findings concerning dual polarization SAR observations are then discussed jointly with a specific limitation of the alternate polarization in Cosmo Sky Med SAR.

* Corresponding author address: Luca Baldini, ISAC-CNR, Via Fosso del Cavaliere, 100, 00133 Roma, Italy; e-mail: l.baldini@isac.cnr.it

## 2. MODELING X-SAR DUAL-POLARIZATION RETURNS IN PRECIPITATION

Models to describe modification induced on SAR surface returns by attenuation and backscattering due to precipitation can be found in the literature (e.g. Atlas et al, 1987, Melshaimer et al. 2001, and Weinman et al., 2008, Fritz and Chandrasekar, 2010, Marzano et al. 2011). The model adopted in this paper can be explained with reference to 1 schematizing a planar wave propagating in a SAR cross-track plane at azimuth *y*. The normalized radar cross section (NRCS) $\sigma^s$ of a surface element Q at ground range *x* is decreased by the 2-way path integrated attenuation (PIA) $l(r)$ caused by the precipitation intervening along the path *r* between Q and SAR antenna and enhanced by the backscattering of the precipitation within the volume sampled by the radar pulse, which, in turn, is attenuated by precipitation between this volume and SAR antenna. The modified NRCS is given by

$$\sigma^0(Q) = \sigma^s(Q,\theta) l[r(x)] + \sin\theta \int_0^{p(x)} \eta(\xi) l[r(\xi)] d\xi \qquad (1)$$

where $\eta$ is the volumetric backscatter cross section ($m^2\ m^{-3}$) of precipitation and $\theta$ is the local incidence angle. Observation geometry is fundamental in determining the resulting NCRS. Backscattering from a surface element close to the point of SAR nearest approach (such as point Q1 in Fig. 1) could not experience precipitation attenuation, but the corresponding radar pulse samples precipitation, determining an increase of the surface backscatter.

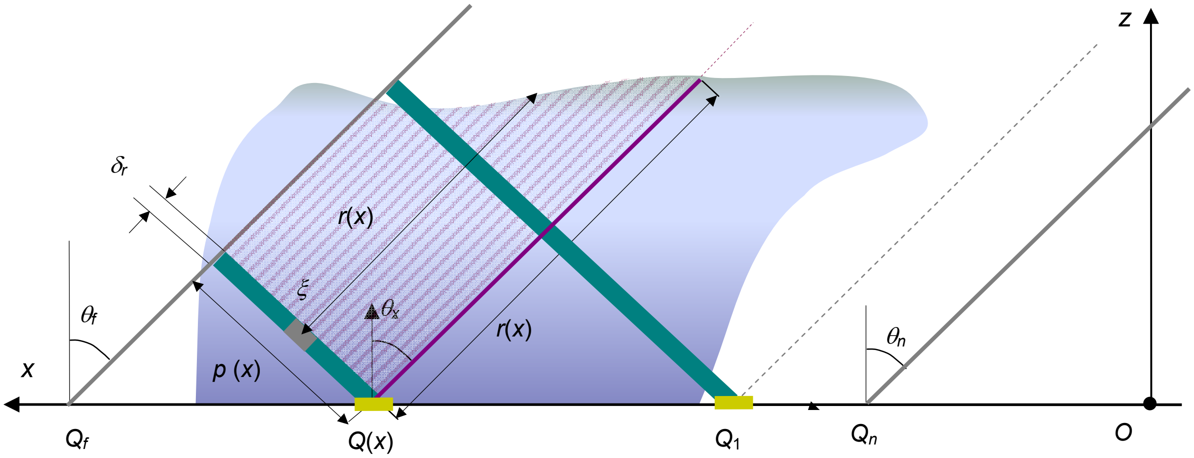


*Figure 1: Cross track geometry of a SAR planar wave passing through a rain cell. $Q_n$ and $Q_f$ are the point of nearest and farthest approach. The backscattering from Q(x) is attenuated along the path r(x) (purple line). Precipitation in the volume identified by the perpendicular to the radial vector in Q determines backscattering attenuated by the precipitation in the shaded area. O is the interception of the cross track plane with the with the SAR ground track*

For a surface element close to the SAR farthest approach point ($Q_f$), no precipitation is sampled by the radar pulse and (1) reduces only to the attenuation term. Over land, at X-band, where both precipitation backscattering and surface backscattering attenuation take place, it is the latter that prevails and rain cells determine black spots SAR images. Parameters in (1) depend on polarization. For clouds and precipitation, polarization characteristics are related to a set of microphysical properties and on the incidence angle of electromagnetic wave (Bringi and Chandrasekar, 2001). Focusing on the linear orthogonal polarizations HH-VV (first letter of the subscript means "receive", the second "transmit") polarization dependency can be made explicit and a parameter $\sigma_D$ (differential NRCS) can be defined as

$$\sigma_D(Q) = \frac{\sigma^s_{HH}\, l_{HH}\left[r(x)\right] + sin\theta \int_0^{p(x)} \eta_{HH}(\xi)\, l_{HH}\left[r(\xi)\right] d\xi}{\sigma^s_{VV}\, l_{VV}\left[r(x)\right] + sin\theta \int_0^{p(x)} \eta_{VV}(\xi)\, l_{VV}\left[r(\xi)\right] d\xi} . \qquad (2)$$

If the terms expressing backscattering enhancement in the numerator and denominator of the (2) are negligible with respect to the attenuation of surface backscattering, $\sigma_D$ can be expressed as $\sigma_D(Q) = \sigma^s_D(Q) l_D\left[r(x)\right]$ where $l_D$ (differential PIA) is the ratio between $l_{HH}$ and $l_{VV}$ and $\sigma^s_D = \sigma^s_{HH} / \sigma^s_{VV}$ . A differential PIA that differs from unit can arise in the presence of propagation effects that are polarization dependent, such as those due to nonspherical oriented hydrometeors like raindrops. Such effects are well recognizable for ground based meteorological radar working at quasi horizontal elevation angles, but are still appreciable even at SAR incidence angles used by the current satellite SAR missions. Cosmo SkyMed features an alternate stripmap polarimetric mode, called Ping Pong that implements strip acquisitions by alternating a pair of transmit/receive polarizations across bursts by mean of the SAR antenna that can be adjusted to be different on transmit and on receive. Since acquisition is performed alternating signal polarization between two of possible ones, only a part of the synthetic antenna length is available in azimuth and the nominal azimuth resolution is consequently reduced. The HH-VV mode, is made of 17 bursts within an image, being 0.15s the time between bursts. The correlation between HH and VV samples in the presence of distributed targets is low and extraction of information on precipitation from complex co-polar correlation coefficient is limited. It is however possible to estimate the differential NRCS as defined by (2).

## 2. USING WEATHER RADAR TO MODEL SAR IMAGES IN PRECIPITATION

Reflectivity bi-dimensional images obtained from ground based weather radar have been successfully used as a ground reference for validating modeling of SAR precipitation observation (Melsheimer et al. 2001, Danklmayer et al. 2009). The use of volumetric weather radar observations to explain observed precipitation backscattering and attenuation effects in SAR images was introduced by Fritz and Chandrasekar (2009) for single polarization S-band weather radars, and later extended to dual-polarization weather radar at S- (Fritz and Chandrasekar, 2010) and C-band (Baldini et al. 2010). Equations (1) and (2) shows that the

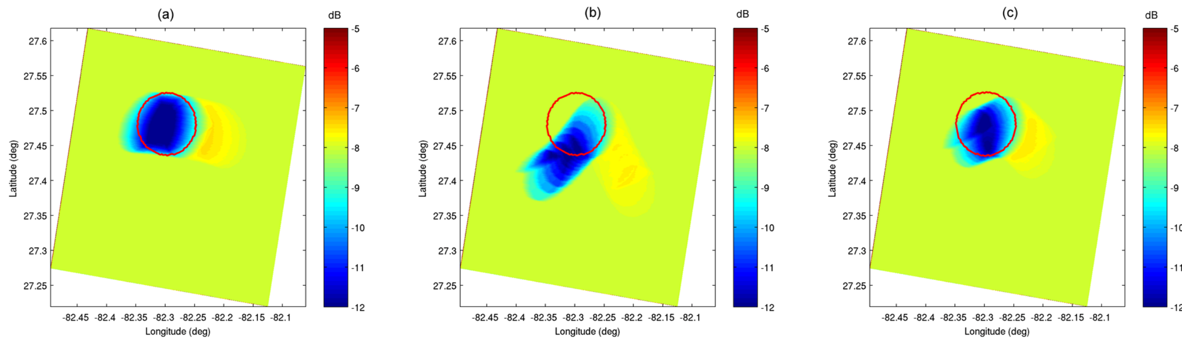


*Figure 2. Deformation induced by reconstructing SAR observation of an idealized cylindrical (represented by the red circle) rain cell moving at 6 km/s (a) using an ideal instantaneous sampling (b) using the geometry of Tampa Bay case and (c) with an optimized radar scan strategy.*

modifications induced by precipitation on surface NRCS at HH and VV polarizations can be estimated if volume reflectivity and the specific attenuation (from which PIA can be computed) associated to each point of the precipitation cell sampled by SAR are known. These two parameters can be estimated using ground based weather radar volume observations. Main steps of the methodology are the following:

a) geometry mapping: SAR and ground radar measurements are referred to a common coordinate system;
b) mapping from measurements at weather radar frequency and elevation angles (usually quasi horizontal) to specific attenuation and volume reflectivity at SAR frequency (namely 9.6 Ghz) and incidence angle.

Concerning the different observation geometries, to compare remote sensing measurements from different platforms, measurements are usually remapped onto a common geographical grid, using also proper interpolation and filtering techniques. Instead, weather radar measurements are mapped onto a 3D grid centered on the point of SAR closest approach. Axes are parallel to the along track and cross track direction and the third axis is determined from orthogonality. In this way each point of a SAR cross track plane is directly mapped onto a local spherical coordinate system of the ground radar. No interpolation in time or in space is performed. The problem arising comparing volume measurements collected typically within a 5-10 minute scan to simulate instantaneous SAR measurements is specifically discussed later. To convert a range profile of radar measurements at a given frequency and elevation angle to the profile that would be observed by a different radar using different frequency and look angle, some techniques are described by Chandrasekar et al. (2006). The adopted method consists in the direct mapping of measurements by the use of simple conversion algorithms established from theoretical modelling that express a measurement in the target frequency as a function of one or more measurements collected by the given weather radar. Relationships are derived using T-matrix simulations (Fritz and Chandrasekar 2011). The conversion process is done by considering separately the effect of frequency from that of viewing angle that has a non-negligible influence for polarization diversity measurements. For the reflectivity factor and specific attenuation at H or V state, the viewing angle dependency has been considered as negligible. Conversely, differential reflectivity is maximum at 0° elevation and decreases as elevation angle $\phi_e$ increases to become null at vertical incidence (Ryzkhov et al. 2005, Bechini et al. 2008). The dependency of differential attenuation and specific differential phase shift $K_{dp}$ can be described in terms of $½(1+\cos 2\phi_e)$. Such relations are used to normalize the weather radar measurements at the 0-degrees elevation and to convert SAR parameters to the given SAR incidence angle. For the Tampa Bay case, all the algorithms to estimate volume reflectivity and specific attenuation are based on reflectivity. Using C-band dual polarization measurements (like in the Piedmont case) specific attenuation at SAR frequency is estimated from $K_{dp}$ at C-band.

### 2.1 Effects of non coincident sampling

SAR and terrestrial weather radar use different observation geometries and different image formation mechanisms: SAR acquisition is quasi instantaneous (5-6 s are needed to collect a 30×30 km image in the PING PONG mode) while an operational weather radar takes up to 10 minutes to collect a volume with an adequate vertical detail and extent. Therefore it is not possible to expect coincidence of measurements especially in the presence of fast-evolving storms. To explain this effect, an idealized rain cell of uniform 40-dBZ reflectivity within a cylinder of 5- km ray and height of 8 km is used. Fig. 2a shows how this cell would result from a SAR at 48° incidence. Geometry parameters are from CSK observations over Tampa Bay (see sect 4). SAR is supposed in a descending orbit, looking right. Reflectivity is supposed to be the same at weather radar

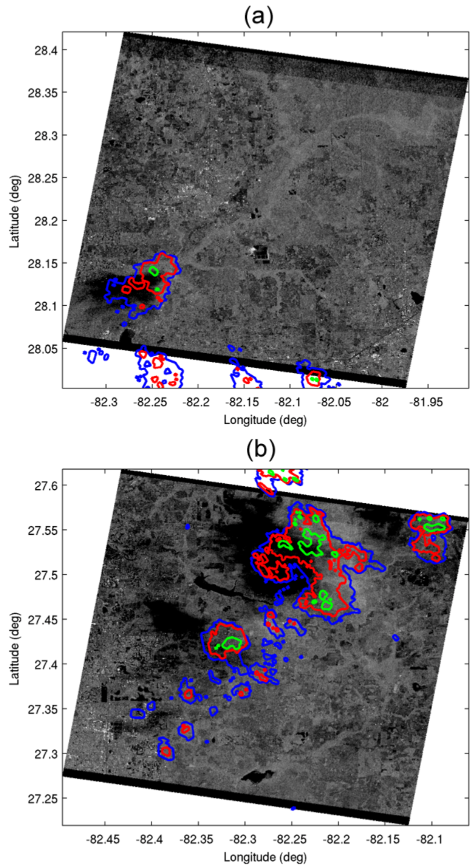


*Figure 3: Images of Tampa Bay collected by CSK2 on (a) 4 July and (b) by CSK1 on 26 June 2010. In blue, red, and green are VMI contours of KTBW radar reflectivity images at 40, 45, and 50dBZ, respectively.*

and SAR frequencies, whereas the specific attenuation at the SAR frequency is estimated through a power law from reflectivity. It can be noticed how SAR observation deforms the shape of the cell that with respect to the circle representing the exact location of the cell. Fig. 2b assumes that cell is moving along a 45° direction with a 6m/s speed and is sampled by an S-band radar using the NEXRAD VCP11 scanning strategy starting at the SAR overpass. Radar is located at latitude and longitude of 27.70° and -82.40°, respectively. A displacement in the direction of the storm velocity is evident as well as an underestimation of the total attenuation with respect to the case of instantaneous sampling. Fig. 2c is obtained using a scanning strategy composed of sector sweeps designed allowing a vertical resolution better then 1 km within the SAR footprint. The methodology was used also to design the radar scan for CSK experiments in Finland. The resulting scan is composed of 14 sector sweeps. Displacement of attenuation is less pronounced than in Fig. 2b and is due both to the reduced acquisition time (160 seconds) and optimized choice of elevations.

## 3. RESULTS

Several CSK acquisitions of sequences of HH-VV ping pong mode images were scheduled over both Piedmont (Italy), Tampa Bay (Florida), and Finland in 2010. CSK constellation was in “Tandem Like” interferometric configuration that allowed acquisitions of the same scene with the same observation geometry (thus reducing the influence of using different incidence angles) and a de-correlation time up to one day between the passages of CSK2 and CSK3 satellites. The data files requested for this work were level 1B single look, uncalibrated, complex images. The hdf 5-formatted CSK files were processed using the Next ESA SAR Toolbox ver. 4A (NEST 4A) for calibration, de-speckling to reduce the spatial resolution from 10×10 $m^2$ to 50×50 $m^2$ and co-registration of different images. Precipitation was recorded by CSK only in Piedmont and in Florida. This paper shows results obtained for the Florida observations using the coincident measurements of the WSR-88D S-band Doppler radar of Tampa Bay (KTBW). CSK images were collected on June 18, 19, 26, and July 4, 12, 20 by all the 3 CSK satellites as strip of 6 adjoining 30x30 $km^2$ images. The incidence angle of CSK was around 48°. Four images contains precipitation, some of them pertaining to Alex, a rare June hurricane developed at the end of June 2010 in the Gulf of Mexico that generated a series of tropical storms over Florida. Analysis focuses on images collected by the satellite CSK1 on June 26 and by satellite CSK2 on July 4. Tampa Bay radio sounding indicates that the 0-degree isothermal was around 5000 and 4400 m for June 26 and July 4, 2010, respectively. NEXRAD analysis does not report hail at ground. KTBW radar were available in term of level II horizontal reflectivity ($Z_h$) with a nominal resolution of 0.5° in azimuth and 0.25 km in range for the first six elevations and 1° in azimuth and 0.500 km for the other. Most of the data were collected using a 14-elevation scanning strategy (0.5, 0.9, 1.3, 1.8, 2.4, 3.1, 4.0, 5.1, 6.4, 8.0, 10.0, 12.5, 15.6, 19.5) repeated every in 5 minutes. Fig. 3 shows two HH images with precipitation, recognizable as dark spots. Simultaneous KTBW radar measurements detect the precipitation cells (see VMI contours of Fig. 3). To reduce the impact of temporal difference between CSK and ground radar acquisitions, SAR observation was reconstructed using, for each elevation, the PPI sweep closest in time to the CSK pass. At the 48-degrees of SAR incidence angle used for the Tampa Bay observations, it is expected that returns and attenuation at HH polarization will be higher than at VV. To this purpose we investigate the

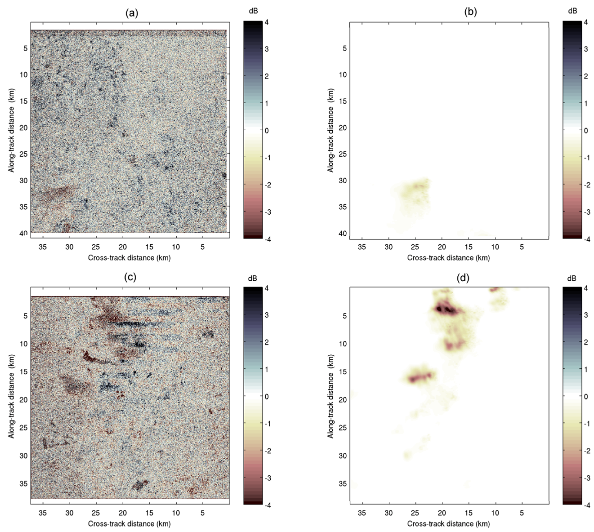


*Figure 4: (a) Difference of $\sigma_D$ of CSK images collected on 4 July (rain) and 20 July 2010 (no rain) and (b) reconstructed differential PIA based on KTBW measurements; (c) and (d) are obtained from 26 June (rain) and 12 June 2010 (no rain) data.*

differential PIA estimated from KTBW radar and the difference $\Delta\sigma_D$ between $\sigma_D$ for a rain image and $\sigma_D$ for a image without rain, close in time and purposely co registered (Fig. 4). $\Delta\sigma_D$ and the differential PIA are in good agreement (artefacts of Fig. 4c are discussed later) for the case of 4 July. ($\Delta\sigma_D$ is computed using the no-rain image of 20 July 2010, co-registered). Images are shown in azimuth-slant range coordinates. Taking into account the expected reduction of spatial resolution due to precipitation (Atlas and Moore 1987), effect of precipitation that reduce SAR spatial resolution, images are resampled to 250x250m$^2$ pixels and resulting $\Delta\sigma_D$ is plotted versus the corresponding NCRS at HH polarization. Negative values of $\Delta\sigma_D$ of the same order of the differential PIA reconstructed from KTBW data

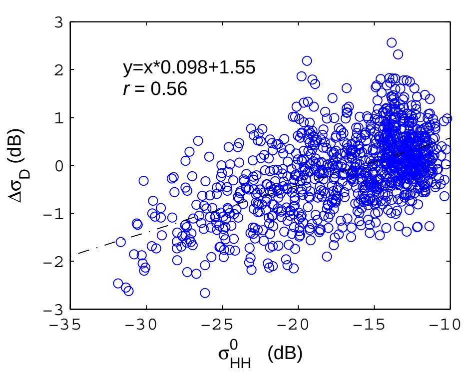


Figur 5: $\Delta\sigma_D$ vs. $\sigma_{HH}$ from CSK measurements of 04 July 2010.

can be found in regions with precipitation (Fig. 5). Fitting dots, a linear relationship can be established as a straightforward consequence of the nearly linear relationship between attenuation and differential attenuation in rain at the CSK frequency. The slope of this linear relation agrees fairly well with that that (0.095) obtained reconstructing the same measurement from KTBW radar. The image of 26 June 2010 instead, presents evident periodic strips that appear as evident in Fig. 4c (see next subsection).

### *4.1 Limitation of Cosmo SkyMed dual polarization*

A specific effect affecting ping pong images is the "scalloping", that is the insurgence of periodic strips, characteristics of burst modes. This effect has been analyzed for SAR burst mode like scanSAR and other SAR alternate polarization implementations (Hawkins and Vigneron 2002). During commissioning phase, ASI has improved the processing system for burst modes with satisfactorily results for most applications (Verdone et al. 2009). However, this effect cannot be completely eliminated. The ground spacing of the scalloping pattern in Fig. 4c is equal to the beam azimuth sweep during the burst cycle period (2.1 km); whereas its depth depends generally on the size of the Doppler mismatch as well as the specific configuration of the processor and imaging system. Mitigation of scalloping requires an accurate estimation of Doppler centroid, which is hampered in the presence of moving targets like precipitation and low signal-to noise-ratio. Precise effects of the residual scalloping that could affect SAR images depend on the details of the actual implementation of the processing chain.

## 5. ACKNOWLEDGMENTS

This work was funded by the Italian Space Agency (ASI, COSMO-SkyMed: Progetti Scientifici N. I/057/09/0 and the NOWCASTING project), NASA Earth and Space Science Fellowship Program - Grant NNX07AO55H, the 2010 Short Term Mobility CNR program. Authors thank Roberto Cremonini and Renzo Bechini (ARPA Piemonte, Italy) and Dmitri Moisseev (University of Helsinki) and for setting up experiments, providing radar data, and assisting in data processing. They acknowledge also the International Cooperation within the NASA PMM Research Program.

## 6. REFERENCES

Agenzia Spaziale Italiana, 2007: *COSMO-SkyMed Mission: COSMO-SkyMed system description & user guide*, (on line: http://www.cosmo-skymed.it/docs/ASI-CSM-ENG-RS-093-A-CSKSysDescriptionAndUserGuide.pdf

Atlas D. and R. K. Moore, 1987. The measurement of precipitation with synthetic aperture radar, *J. Atmos. Ocean Tech.* **4** ,), pp 368–376.

Baldini L., Fritz J., Gorgucci E., and V. Chandrasekar, Interpretation of satellite observations of precipitation using C-band polarimetric radar data, *Proc. 6th European Conf. on Radar in Meteorology and Hydrology*, Sibiu, Romania, Sep. 2010.

Chandrasekar, V., S. Lim, E. Gorgucci, 2006. Simulation of X-band rainfall observations from S-band radar data. J. Atmos. Oceanic Technol., 23, 1195–1205.

Danklmayer A., B. Dueoring, M. Schwerdt, and M. Chandra, 2009. Assessment of atmospheric propagation effects in SAR images, IEEE Trans. Geosci. Remote Sensing, 47, 3507–3518.

Fritz J. and V. Chandrasekar, 2010: Simultaneous observations and analysis of severe storms using polarimetric X-band SAR and ground-based weather radar, IEEE Trans. Geosci. Remote Sensing, 48, 10-22.

Fritz J. and V. Chandrasekar, 2011: Simulating polarimetric radar observations of mie scattering hydrometeors from lower frequency measurements, submitted to AMS J. Atmos. Ocean Tech.

Hawkins R. K. and P. Vachon, 2002. Modeling SAR scalloping in burst mode products from RADARSAT-1 and ENVISAT, in *Proc. CEOSWorkshop on SAR, London, U.K.*, ESA Pub. SP-520.

Marzano F. S., S. Mori, M. Chini, L. Pulvirenti, N. Pierdicca, M. Montopoli, and J. A. Weinman, 2011. Potential of high-resolution detection and retrieval of precipitation fields from X-band spaceborne synthetic aperture radar over land, Hydrol. Earth Syst. Sci., 15, 859-875,

Ryzhkov, V. R., S. E. Giangrande, V. M. Melnikov, and T. J. Schuur, 2005: Calibration issues of dual-polarization radar measurements. J. Atmos. Oceanic Technol., 22, 1138-1155.

Verdone G. R., Viggiano R., Lopinto E., Milillo G., Candela L., Lombardi N., and V Giannini, 2009 Processing algorithms for COSMO-SkyMed SAR Sensor, *Proc. of IGARSS 2009*, pp.II-2771-II-2774.

Weinman J. A. and F. S. Marzano, 2008. An exploratory study to derive rainfall over land from spaceborne synthetic aperture radars, J. Appl. Meteorol. Climatol., 47, 562–575.